Combustion and Flame 284 (2026) 114654

Contents lists available at ScienceDirect

Combustion and Flame

journal homepage: www.sciencedirect.com/journal/combustion-and-flame

# A reduced model of smoldering-to-flaming (StF) transition

Pichayaporn Viriya-amornkij [a], Kazunori Kuwana [a,*], Yasuhisa Saito [b], Xinyan Huang [c]

[a] Department of Global Fire Science and Technology, Tokyo University of Science, 2641 Yamazaki, Noda, Chiba 278-8510, Japan
[b] Department of Mathematics, Shimane University, 1060 Nishikawatsucho, Matsue, Shimane 690-8504, Japan
[c] Department of Building Environment and Energy Engineering, The Hong Kong Polytechnic University, 181 Chatham Road South, Kowloon, Hong Kong

ARTICLE INFO

*Keywords:*
Smoldering
Smoldering-to-flaming transition (StF)
Flaming
Reduced model
Extinction

ABSTRACT

This study proposes a reduced model to predict the smoldering-to-flaming (StF) transition. Three chemical reactions, including surface and gas-phase reactions, are considered, coupled with heat and mass transfer between the surface and the gas phase. Unknown quantities, such as surface/gas-phase temperatures, reaction rates, and species concentrations, are solved simultaneously as part of the solution with pure smoldering, pure flaming, and combined cases, demonstrating the simplicity yet wide applicability of the model. Dimensionless parameters are first introduced to simplify the equations and to illustrate the nature of the model's solutions. The results show an increase in temperature with the oxygen mass fraction, along with a higher surface temperature than the gas-phase temperature in smoldering mode and vice versa in flaming mode. The combined case predicts the shift from steady smoldering to steady flaming, indicating the critical temperature and species concentrations at the spontaneous StF transition. Combustion maps consisting of smoldering, bistable, and flaming regimes are constructed over a range of oxidizer flow rates. With an increase in oxidizer flow rate, the upper limit of oxygen mass fraction for smoldering and the lower limit of oxygen mass fraction for flaming initially decrease, reach a minimum, and then increase with oxidizer flow rate, while the lower limit of oxygen mass fraction for smoldering has a broader boundary and decreases with the oxidizer flow rate. These limits shift to higher oxygen mass fractions when increasing heat loss. The model is then validated against previous experimental data and applied to further investigate the effects of external radiant heat flux. The lower limit of oxygen mass fraction for flaming decreases with increasing external radiant heat flux, while the surface temperature remains within a certain range.

## 1. Introduction

Smoldering fires pose a serious hazard in both residential, industrial, and wildland settings, as they emit high levels of toxic compounds, are challenging to detect due to their flameless characteristics, and can be initiated by weak heat sources [1]. They may extinguish under conditions of limited oxygen supply (smothering) or high convective airflow (blowoff) [2,3]. However, they also have the potential to transition into more intense flaming fires under certain conditions, such as an excessive oxygen supply [4–7], high heat flux [8], and large airflow velocity [9,10]. This smoldering-to-flaming (StF) transition is a gas-phase ignition process in which heterogeneous reactions act as a source of both fuel and elevated temperature [11]. It is hypothesized that the high-temperature char oxidation can pilot the pyrolysis gas mixture, triggering the StF transition [12,13]. Although this fundamental combustion issue has been studied experimentally and theoretically, there remains a lack of simple yet broadly applicable models to describe the StF transition phenomenon.

The spontaneous transition from smoldering to flaming (StF) was often experimentally investigated under various oxidizer flow rates. For example, Ohlemiller et al. [10] reported a StF transition in cellulosic insulation at a minimum velocity of 5 m/s for reverse smoldering and 2 m/s for forward smoldering. Tse et al. [11] found that the StF transition of polyurethane (PU) foam occurred inside the hot char region, where the formation of the large pore promoted the onset of gas-phase reactions. The effects of oxygen concentration and external radiant heat flux on the StF transition were studied by Bar-Ilan et al. [7] and Putzeys et al. [5,6]. A simplified energy balance analysis is proposed to predict the transition boundaries and char oxidation velocity. The StF transition can also be initiated by a piloted source, like a typical piloted flame ignition. Putzeys et al. [6] reported the piloted ignition of gaseous products at a minimum oxygen mole fraction of 0.17 under the external radiant heat flux of 8.75 kW/m$^2$ for non-fired retarded PU foam.

* Corresponding author.
*E-mail address:* kuwana@rs.tus.ac.jp (K. Kuwana).

https://doi.org/10.1016/j.combustflame.2025.114654
Received 30 June 2025; Received in revised form 17 November 2025; Accepted 18 November 2025
Available online 11 December 2025

**Nomenclature**

| | |
|---|---|
| $B_i$ | pre-exponential factor of reaction $i$ [balance] |
| $c$ | specific heat capacity [J/kg K] |
| $D$ | mass diffusivity [$m^2$/s] |
| $E_i$ | activation energy of reaction $i$ [J/mol] |
| $h$ | heat transfer coefficient [W/$m^2$ K] |
| $h_m$ | mass transfer coefficient [kg/$m^2$ s] |
| $Q_i$ | heat of reaction $i$ [J/kg] |
| $Q_{ext}$ | external radiant heat flux [W/$m^2$] |
| $R$ | universal gas constant [J/mol K] |
| $S$ | char surface area [$m^2$] |
| $T$ | temperature [K] |
| $v$ | oxidizer flow rate [$m^3$/s] |
| $V$ | gas-phase volume [$m^3$] |
| $Y_j$ | mass fraction of species $j$ [–] |

*Greek symbols*

| | |
|---|---|
| $\alpha$ | thermal diffusivity [$m^2$/s] |
| $\nu_{i,j}$ | mass-based stoichiometric coefficients of species $j$ in reaction $i$ [kg/kg] |
| $\rho$ | bulk density [kg/$m^3$] |
| $\dot{\omega}_i''$ | rate of heterogeneous reaction $i$ [kg/$m^2$ s] |
| $\dot{\omega}_i'''$ | rate of homogeneous reaction $i$ [kg/$m^3$ s] |

*Subscripts*

| | |
|---|---|
| 0 | inlet value |
| C | char |
| CO | carbon monoxide |
| $CO_2$ | carbon dioxide |
| crit | critical value |
| fl | lower limit of flaming |
| g | gas phase |
| max | maximum |
| $O_2$ | oxygen |
| s | surface |
| sml | lower limit of smoldering |
| smu | upper limit of smoldering |

The complex chemistry and limited understanding of heat and mass transfer between the solid and gas phases complicate the modeling of the StF transition. Dodd et al. [14] conducted the 2-D computational fluid dynamics (CFD) simulations of the StF transition in PU foam, following the experiments performed by [5,7]. By considering seven heterogeneous reactions and one homogeneous reaction, they simulated both forward and opposed smoldering spread and also its transition to flaming under different heat fluxes, air velocities, and oxygen concentrations. They found that the global gas-phase oxidation played a major role in the StF transition. Subsequently, Yang et al. [15] also conducted a 2-D CFD simulation with three heterogeneous reactions and one global homogenous gas-phase reaction to simulate the experiment conducted by [10]. They concluded that the hotter surface char layer acts as an ignition source for heating the gas mixture, and both pyrolysis and char-oxidation reactions behave like a gaseous fuel supplier for the gas-phase reaction.

Despite advancements in the CFD modeling of the StF transition, a gap appears to exist between simplified theoretical and detailed numerical models. Previously, Kadowaki et al. [4] proposed a one-dimensional (1-D) smoldering model that reproduced increased smoldering rate and temperature with higher oxygen concentrations. The turning points obtained from the solutions indicated the extinctions under lower oxygen concentrations. The StF transition at high oxygen concentrations was predicted by considering a gas-phase reaction with an infinite char-oxidation rate. Nevertheless, a 1-D steady flaming solution cannot be determined because oxygen is consumed in the flame, leaving no oxygen available to react with the char within their reaction model. Then, the accumulation of char invalidates the steady-state assumption. As shall be seen later in this paper, obtaining the steady flaming branch of the solution is essential for predicting the bistable regime, where both steady flaming and steady smoldering are possible, as experimentally observed by [16,17].

Based on the above background, this study proposes a reduced model that considers the mass, species, and energy balance within the gas phase and at the char surface. The model aims to predict the temperature, species concentrations for each mode of combustion, as well as its limits. The effects of oxygen mass fraction, oxidizer flow rate, and heat loss on StF transition are investigated. Furthermore, the predicted results are validated against previously reported experimental data.

## 2. Theoretical model

### 2.1. Model description

A reduced model proposed in this study is inspired by the concept that the StF transition occurs in the pore region generated by char oxidation when the char surface temperature becomes high enough to spontaneously ignite the combustible gas mixture [5,7,11]. Based on previous experimental observations, the key mechanism of transition is the competition between the surface char oxidation and the gas-phase combustion reactions; thus, the model does not refer to any specific configuration but instead focuses on the auto-ignition of the gas phase by the hot char surface. The pyrolysis reaction is also disregarded for simplicity. In reality, the endothermic pyrolysis reaction plays a similar role to heat loss, and the assumption of neglecting it influences the condition of the StF transition. However, the essential mechanism for the StF transition is the char-oxidation reaction [5]. A schematic diagram of the model is illustrated as shown in Fig. 1.

The surface char-oxidation reaction produces gases and ash as products [13]. Sega et al. [18] measured the species concentrations of smoldering rolled paper and found that CO oxidation is the dominant chemical reaction driving spontaneous ignition, due to the lower concentrations of $CH_4$ and $H_2$. Later, Yamazaki et al. [19] adopted this assumption and introduced a solid-phase model by considering the global char-oxidation reaction. Following a similar approach, the present study considers only CO as the product of the char-oxidation reaction (R1). It should be noted that neglecting $CO_2$ production and other volatile species may lead to an earlier prediction of the StF transition, resulting in lower predicted oxygen concentration thresholds. Although the present model could incorporate $CO_2$ production, doing so would increase the number of model parameters and require adjustment of the

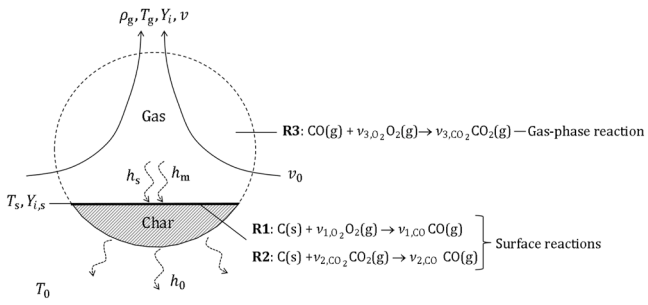


**Fig. 1.** Schematic diagram of the reduced model.

kinetic parameters. Therefore, in this paper, only CO is considered as the product.

Three different cases are tested in this paper: (1) pure smoldering case, (2) pure flaming case, and (3) combined case. In the pure smoldering case, only smoldering reaction (R1) is included: char reacts with $O_2$ at the char surface, producing CO in the gas phase. In the pure flaming case (R1 is excluded, while R2 and R3 are included), CO reacts with $O_2$ in the gas phase to produce $CO_2$, which subsequently reacts with the char. In the combined case, all three reactions (R1, R2, and R3) are included to capture both smoldering and flaming reactions, as well as the transition between them.

The extinction phenomenon is significantly influenced by heat loss. The StF transition, which is the main focus of this paper, is expected to be strongly influenced by heat loss from the smoldering char surface to the surroundings. This is because the surface temperature is higher than the gas-phase temperature within the smoldering combustion. This effect is therefore considered in the present model through the heat transfer coefficient $h_0$.

The following assumptions are made to simplify the equations.

1) The temperature and species mass fraction distributions within the gas phase are represented by two values, i.e., the bulk and the surface quantities, which are connected through heat and mass transfer coefficients.
2) The global reaction rates are assumed to be first order with respect to each reactant. Consideration of global reaction mechanisms requires adjustment of kinetic parameters depending on the purpose of the analysis. However, in this study, we adopt a global reaction mechanism for the sake of simplicity. The reaction rates of R1, R2, and R3 are expressed in the following forms:

$$\dot{\omega}_1'' = B_1 \rho_C \rho_g Y_{O_2,s} \exp\left(-\frac{E_1}{RT_s}\right) \tag{1}$$

$$\dot{\omega}_2'' = B_2 \rho_C \rho_g Y_{CO_2,s} \exp\left(-\frac{E_2}{RT_s}\right) \tag{2}$$

$$\dot{\omega}_3''' = B_3 \rho_g^2 Y_{CO} Y_{O_2} \exp\left(-\frac{E_3}{RT_g}\right) \tag{3}$$

3) The temperatures and mass fractions in the gas and solid phases are related through the heat and mass transfer between them. There is no gas diffusion through the char region.
4) All material properties, including gas density, are assumed to be constant.
5) There is no shrinkage or change in volume due to the reactions or heating, i.e., a quasi-steady state is assumed.

### 2.2. Conservation equations

The model considers the mass, species, and energy balance in the gas phase and at the char surface with two surface reactions (R1 and R2) and one gas-phase reaction (R3).

The dimensionless form of the mass balance in the gas phase is shown in Eq. (4). The dimensionless quantities are normalized using the inlet values, which will be described later.

$$1 + \bar{\dot{\omega}}_1'' + \bar{\dot{\omega}}_2'' = \bar{v} \tag{4}$$

The species balance of $O_2$, CO, and $CO_2$ in the gas phase are expressed in the dimensionless forms in Eqs. (5)-(7), respectively.

$$Y_{O_2,0} - \bar{h}_m\left(Y_{O_2} - Y_{O_2,s}\right) - \nu_{3,O_2}\bar{\dot{\omega}}_3''' = \bar{v} Y_{O_2} \tag{5}$$

$$-\bar{h}_m\left(Y_{CO} - Y_{CO,s}\right) - \nu_{3,CO}\bar{\dot{\omega}}_3''' = \bar{v} Y_{CO} \tag{6}$$

$$-\bar{h}_m\left(Y_{CO_2} - Y_{CO_2,s}\right) + \nu_{3,CO_2}\bar{\dot{\omega}}_3''' = \bar{v} Y_{CO_2} \tag{7}$$

where $Y_{O_2,0}$ is the ambient oxygen mass fraction; the influence of this parameter will be tested in Section 3.

The species balance of $O_2$, CO, and $CO_2$ at the char surface is expressed in Eqs. (8)-(10), respectively.

$$\bar{h}_m\left(Y_{O_2} - Y_{O_2,s}\right) - \nu_{1,O_2}\bar{\dot{\omega}}_1'' = 0 \tag{8}$$

$$\bar{h}_m\left(Y_{CO} - Y_{CO,s}\right) + \nu_{1,CO}\bar{\dot{\omega}}_1'' + \nu_{2,CO}\bar{\dot{\omega}}_2'' = 0 \tag{9}$$

$$\bar{h}_m\left(Y_{CO_2} - Y_{CO_2,s}\right) - \nu_{2,CO_2}\bar{\dot{\omega}}_2'' = 0 \tag{10}$$

The energy balance in the gas phase, Eq. (11), accounts for the sensible heat of the fresh air, the heat generated by R3, and the heat transfer between gas phase and char surface.

$$1 - \bar{h}_s\left(\bar{T}_g - \bar{T}_s\right) + \bar{Q}_3\bar{\dot{\omega}}_3''' = \bar{v}\bar{T}_g \tag{11}$$

The energy balance at the char surface, as expressed in Eq. (12), illustrates the balance between the heat transfer to the char surface, heat lost to the surroundings, the heat generated by R1 and R2, and the external radiant heat flux (if any).

$$\bar{h}_s\left(\bar{T}_g - \bar{T}_s\right) - \bar{h}_0\left(\bar{T}_s - \bar{T}_0\right) + \bar{Q}_1\bar{\dot{\omega}}_1'' + \bar{Q}_2\bar{\dot{\omega}}_2'' + \bar{Q}_{ext} = 0 \tag{12}$$

The following summarize the dimensionless quantities normalized using inlet values:

$$\begin{aligned}
\bar{v} &= v/v_0,\ \bar{T}_g = T_g/T_0,\ \bar{T}_s = T_s/T_0,\\
\bar{E}_i &= E_i/RT_0,\ \bar{Q}_i = Q_i/c_g T_0,\\
\bar{Q}_{ext} &= SQ_{ext}/\rho_g c_g v_0 T_0,\ \bar{h}_s = Sh_s/\rho_g c_g v_0,\\
\bar{h}_0 &= Sh_0/\rho_g c_g v_0,\ \bar{h}_m = Sh_m/\rho_g v_0,\\
\bar{B}_1 &= SB_1\rho_c/v_0,\ \bar{B}_2 = SB_2\rho_c/v_0,\ \bar{B}_3 = VB_3\rho_g/v_0,\\
\bar{\dot{\omega}}_1'' &= S\dot{\omega}_1''/\rho_g v_0,\ \bar{\dot{\omega}}_2'' = S\dot{\omega}_2''/\rho_g v_0\\
\bar{\dot{\omega}}_3''' &= V\dot{\omega}_3'''/\rho_g v_0
\end{aligned} \tag{13}$$

The nine conservation equations for mass, species, and energy in the gas and solid phases, Eqs. (4)-(12), are employed to solve the following nine dimensionless variables: $\bar{v}$, $\bar{T}_g$, $\bar{T}_s$, $Y_{O_2}$, $Y_{O_2,s}$, $Y_{CO}$, $Y_{CO,s}$, $Y_{CO_2}$, and $Y_{CO_2,s}$. To solve the system of non-linear equations, we utilized the scipy.optimize.root function available in the SciPy library.

## 3. Results and discussion

In this section, the predicted temperatures by pure smoldering, pure flaming, and combined cases, calculated using the dimensionless parameters listed in Table 1, are first introduced to highlight the nature of the model's solutions and to test the effects of oxygen mass fraction, oxidizer flow rate, and heat loss on StF transition. Then, the model is validated against the previous experimental data [6] at several oxygen mass fractions, and radiant heat fluxs.

### 3.1. Dimensionless solutions

The predicted $\bar{T}_g$, $\bar{T}_s$, and $\bar{T}_{max} = \max(\bar{T}_g, \bar{T}_s)$ as a function of $Y_{O_2,0}$ are shown in Fig. 2. Note that the parameter values (Table 1) are not associated with any particular cases, and Fig. 2 is to illustrate the model's capability. The solid lines represent the gas-phase temperature ($\bar{T}_g$), while the dashed lines show the surface temperature ($\bar{T}_s$). Fig. 2(a) illustrates the solutions of the pure smoldering case. The black lines represent the stable branch, while the gray lines indicate the unstable solutions that lack physical meaning. We consider the eight-dimensional dynamical system for $Y_{O_2}$, $Y_{O_2,s}$, $Y_{CO}$, $Y_{CO,s}$, $Y_{CO_2}$, $Y_{CO_2,s}$, $\bar{T}_g$, and $\bar{T}_s$. The stability of a steady-state solution is analyzed by numerically evaluating

**Table 1**
Dimensionless parameters used in Figs. 2–5.

| Parameters | Value |
|---|---|
| $\bar{B}_1$ | $2 \times 10^{14}$ |
| $\bar{E}_1$ | 50 |
| $\bar{B}_2$ | $2 \times 10^{14}$ |
| $\bar{E}_2$ | 50 |
| $\bar{B}_3$ | $2 \times 10^{8}$ |
| $\bar{E}_3$ | 50 |
| $\bar{h}_s$ | 6 |
| $\bar{h}_0$ | 6 |
| $\bar{Q}_1$ | 60 |
| $\bar{Q}_2$ | −50 |
| $\bar{Q}_3$ | 30 |
| $\bar{Q}_{ext}$ | 0 |
| $\bar{h}_m$ | 6 |

the eigenvalues of the 8 × 8 Jacobian matrix, based on Eqs. (5)-(12). A solution is considered stable if all of its eigenvalues have negative real parts [20,21].

The results show that $\overline{T}_s$ is higher than $\overline{T}_g$, confirming the characteristic of smoldering combustion, where surface temperature is higher than gas-phase temperature. Both temperatures increase with increasing $Y_{O_2,0}$. Extinction occurs at $Y_{O_2,0} = 0.12$, where the upper and lower branches merge, representing a turning point below which the upper-branch solution ceases to exist. The concept of a turning point associated with extinction and ignition was previously introduced in premixed and diffusion flame theory [22,23].

The pure flaming case is shown in Fig. 2(b), characterized by a higher $\overline{T}_g$ than $\overline{T}_s$. The extinction is found at $Y_{O_2,0} = 0.32$ for the flaming reaction.

As smoldering is characterized by a higher $\overline{T}_s$ than $\overline{T}_g$ and flaming by a higher $\overline{T}_g$ than $\overline{T}_s$, StF conditions can be conveniently identified by plotting $\overline{T}_{max} = \max(\overline{T}_g, \overline{T}_s)$ of the combined case, as shown in Fig. 2(c) with the white squares ($\overline{T}_{max} = \overline{T}_s$) and black circles ($\overline{T}_{max} = \overline{T}_g$). Different regimes of extinction, smoldering, bistable, and flaming are identified. In the smoldering regime, $0.12 < Y_{O_2,0} < 0.33$, the only stable solution is smoldering. When $0.33 < Y_{O_2,0} < 0.37$, both flaming and smoldering are stable, characterizing a bistable regime. If an additional ignition source, such as an open flame or spark ignition, is applied to the system, flaming can be initiated, as experimentally observed by [17]. When $Y_{O_2,0} > 0.37$, the spontaneous StF transition occurs because there is no stable smoldering solution. $\overline{T}_{max}$ shifts from $\overline{T}_s$ to $\overline{T}_g$, indicating that the gas-phase reaction becomes dominant and the system fully transitions into the flaming regime. In the condition of Fig. 2(c), StF coincided with the point of $\overline{T}_g = \overline{T}_s$, an equivalent condition to the adiabaticity criterion discussed in [4].

$Y_{CO}$ as a function of $Y_{O_2,0}$ is plotted in Fig. 3, showing that $Y_{CO}$ is produced by surface reaction R1 within the smoldering regime. Once the StF transition occurs, $Y_{CO}$ decreases as it is consumed by the gas-phase reaction R3.

The effect of oxidizer flow rate on gaseous products and combustion mode is investigated, as shown in Figs. 4 and 5, respectively. Given that $v_0^*$ is the base oxidizer flow rate used to nondimensionalize the parameters in Figs. 2 and 3, the dimensionless expression of $v_0/v_0^*$ is introduced to represent the changes in the oxidizer flow rate. The gas-phase mass fractions and gas-phase temperature at the critical StF point in the smoldering branch are shown in Fig. 4. $Y_{CO,crit}$ decreases with increasing $v_0/v_0^*$, in contrast to $Y_{O_2,crit}$ and $T_{g,crit}$, which increase with $v_0/v_0^*$. $Y_{CO_2,crit}$ remains relatively low throughout the entire range of $v_0/v_0^*$. The inverse trend between $Y_{CO,crit}$ and $T_{g,crit}$ indicates that both CO concentration and gas-phase temperature are important factors in triggering the transition. When $Y_{CO,crit}$ is low, a higher $T_{g,crit}$ is required to initiate the gas-phase reaction, whereas a lower $T_{g,crit}$ is sufficient $Y_{CO,crit}$ is high.

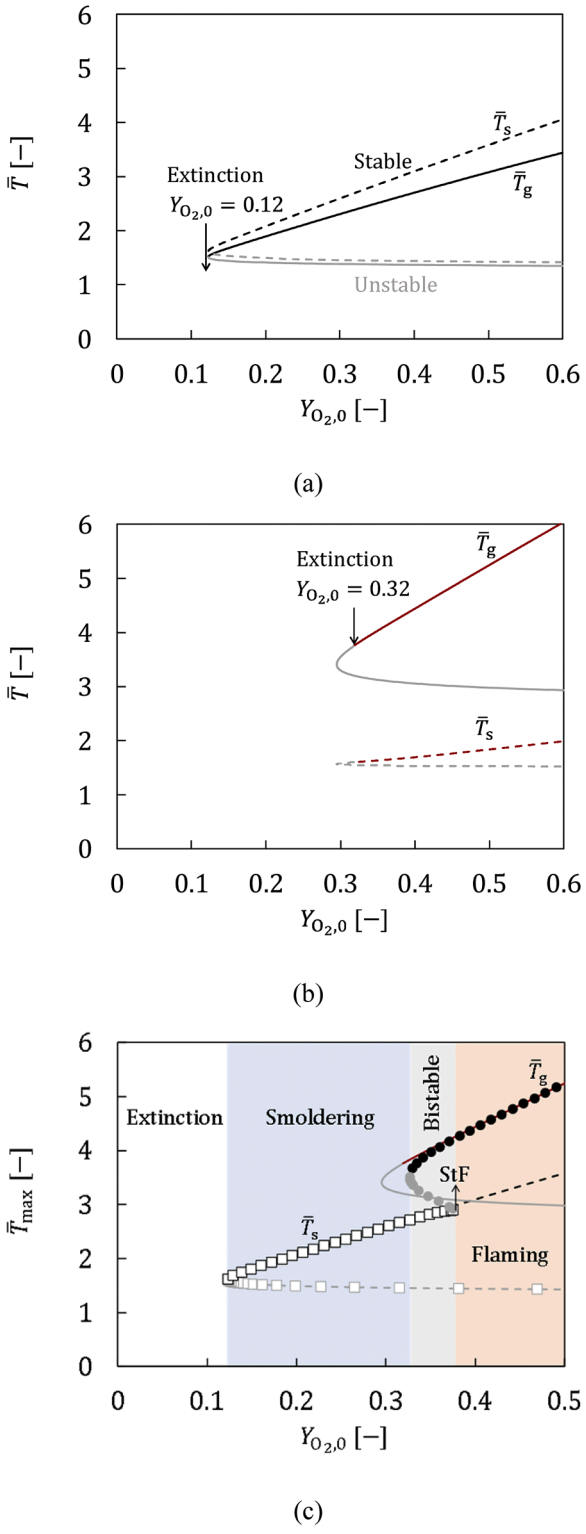


**Fig. 2.** Predicted dimensionless temperature for (a) pure smoldering case, R1, (b) pure flaming case, R2+R3, and (c) combined case, R1+R2+R3. Black color: stable solution; Gray color: unstable solution; Dashed line: predicted $\overline{T}_s$ (pure smoldering case); Solid line: predicted $\overline{T}_g$ (pure flaming case); □: predicted $\overline{T}_s$ (combined case); ●: predicted $\overline{T}_g$ (combined case); $v_0^* = 4.2 \times 10^{-7}$ m$^3$/s.

In Fig. 5, the blue line represents the lower limit of oxygen mass fraction for smoldering ($Y_{O_2,0,sml}$) at a given $v_0/v_0^*$. No smoldering combustion can sustain below $Y_{O_2,0,sml}$. The red line indicates the upper limit of oxygen mass fraction for smoldering ($Y_{O_2,0,smu}$), beyond which

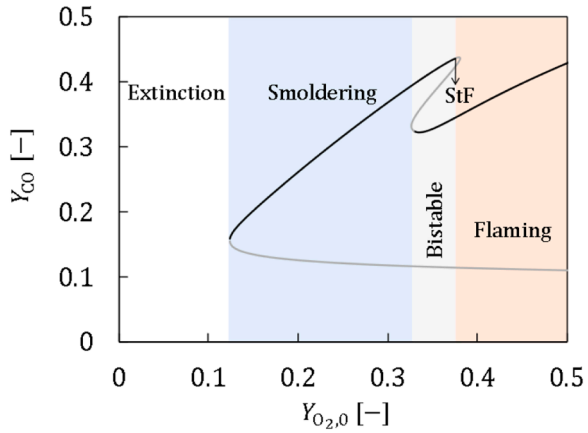


**Fig. 3.** Predicted CO mass fractions ($Y_{CO}$) by a combined case. Black color: stable solution; Gray color: unstable solution; $v_0^* = 4.2 \times 10^{-7}$ m$^3$/s.

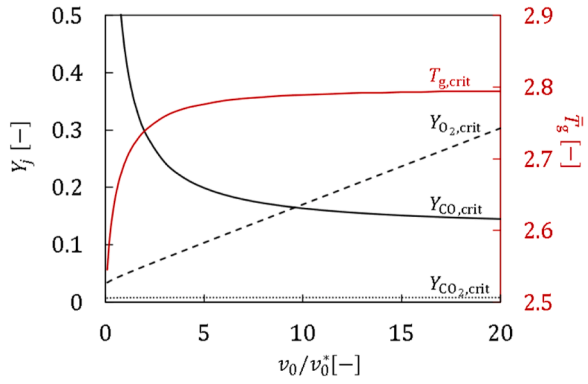


**Fig. 4.** Gas-phase species mass fractions ($Y_j$) and gas-phase temperature ($T_g$) at the critical StF transition as functions of normalized oxidizer flow rates ($v_0$ /$v_0^*$).

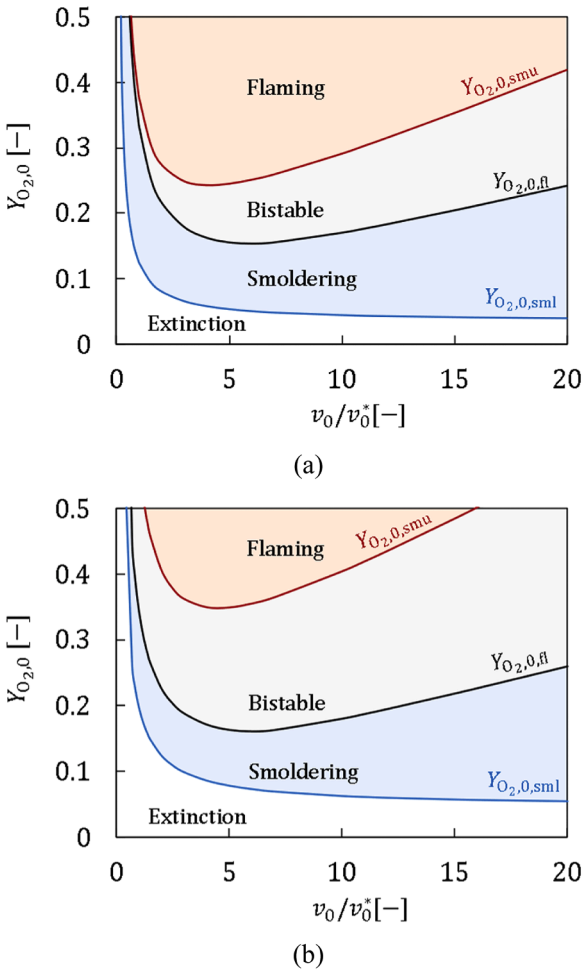


**Fig. 5.** Dependence of combustion mode on normalized oxidizer flow rate ($v_0/v_0^*$). (a) $\bar{h}_0 = 6$, (b) $\bar{h}_0 = 10$. Blue line: lower limit of oxygen mass fraction for smoldering ($Y_{O_2,0,sml}$) Black line: lower limit of oxygen mass fraction for flaming ($Y_{O_2,0,fl}$); Red line: upper limit of oxygen mass fraction for smoldering ($Y_{O_2,0,smu}$).

only flaming combustion is possible. In other words, the spontaneous StF transition occurs when $Y_{O_2,0} = Y_{O_2,0,smu}$. The black line shows the lower limit of oxygen mass fraction for flaming ($Y_{O_2,0,fl}$), below which flaming reactions cannot be sustained.

Fig. 5(a) represents the case of $\bar{h}_0 = 6$, showing that $Y_{O_2,0,smu} > Y_{O_2,0,fl} > Y_{O_2,0,sml}$ throughout the range of $v_0/v_0^*$. The broader lower limit of smoldering compared to flaming confirms its ability to sustain under extreme conditions, highlighting the hidden danger of smoldering combustion. With increasing $v_0$, the flaming combustion becomes harder to ignite, as it does at very low $v_0$ due to the balance between oxygen supply and convective heat loss. Both $Y_{O_2,0,fl}$ and $Y_{O_2,0,smu}$ initially decrease, reaching a minimum value of approximately $Y_{O_2,0,fl} \approx 0.15$ and $Y_{O_2,0,smu} \approx 0.24$ at $v_0/v_0^* \approx 4$ and 6, respectively, before starting to increase again with $v_0/v_0^*$. This minimum oxygen concentration is significant from a fire safety perspective, as it represents the condition under which combustion is most easily initiated. A similar trend of initially decreasing $Y_{O_2,0,fl}$ with $v_0/v_0^*$ was experimentally reported by [16]. Within the range of $v_0/v_0^*$ considered in this study, no smoldering reaction can be observed at any $v_0/v_0^*$ below $Y_{O_2,0,sml} \approx 0.04$.

Fig. 5(b) shows the results when increasing $\bar{h}_0$ to 10. It can be seen that the lower limits of each combustion mode shift to the higher values, especially in the flaming regime. Again, the parameters used for Fig. 5 do not reflect any particular cases; the results shown in this figure should be understood as those qualitatively illustrating the model's capability.

### 3.2. Model validation

A brief description of the piloted ignition experiment on the smoldering gaseous products conducted by Putzeys et al. [6] is first provided here. PU foam was placed in an upward wind tunnel under various oxygen mole fractions between 0.15 and 0.35 and an external radiant heat flux between 7.25 and 8.75 kW/m$^2$. The radiant heat flux was applied to supply the additional heat to the sample and counter the convective heat losses on the free surface. Each test started by initiating the smoldering spread at the bottom end of the sample. Then, pilot ignition was activated once the smoldering reaction had propagated. Note that the activation of pilot ignition is not a spontaneous StF phenomenon but rather a typical piloted ignition of the gaseous products. The experimental data in [6] were used for comparison due to the limited

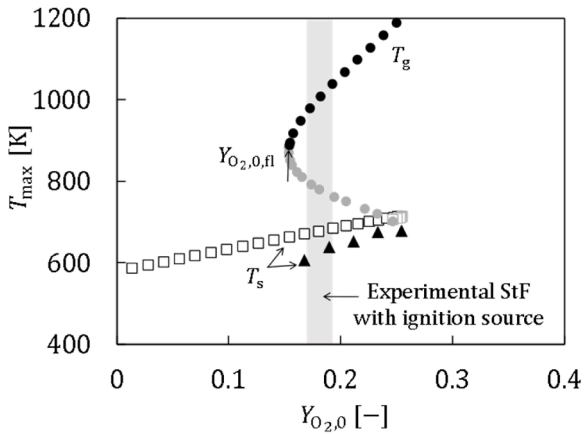


**Fig. 6.** Validation with the experiment. Black color: stable solution; Gray color: unstable solution; □: predicted $T_s$ (combined case); ●: predicted $T_g$ (combined case); ▲: experimental $T_s$ [6]; $v_0^* = 4.2 \times 10^{-7}$ m$^3$/s.

availability of auto StF data, which mainly focuses on the flame spread rate that is beyond the scope of the model in the present study. In the future, more detailed analysis will be necessary; for example, combining our model with CFD simulations may help improve the model's capability. From [6], the critical oxygen mass fraction capable of igniting the flame corresponds to $Y_{O_2,0,fl}$ in Fig. 5, where flaming combustion can be initiated if there is a sufficiently strong ignition source. Experimental $T_s$ with an external radiant heat flux of 8.75 kW/m$^2$ is plotted as a function of $Y_{O_2,0}$, as shown with the black triangles in Fig. 6. The flaming combustion was ignited at $Y_{O_2,0} = 0.19$, while no ignition occurred at $Y_{O_2,0} = 0.17$. The critical condition is, therefore, within the gray shaded area.

The predicted $T_{max}$ is calculated using the parameters listed in Table 2 and shown by the white squares ($T_{max} = T_s$) and black circles ($T_{max} = T_g$) in Fig. 6. The sensitivity analysis of the parameters in Table 2 is conducted as shown in Appendix A. The external radiant heat flux ($Q_{ext}$) of 8.75 kW/m$^2$ is included in the energy balance equation at the char surface, Eq. (12). A reasonable agreement between the predicted and experimental data is confirmed, showing an increase in $T_s$ with $Y_{O_2,0}$. The predicted $Y_{O_2,0,fl}$ is 0.16, which is slightly underpredicted; however, considering the simplicity of the model, it aligns reasonably well with the experimental data. Note that the dimensional values of heat and mass transfer coefficients depend on several factors, such as

**Table 2**
Dimensional parameters used in Figs. 6–8.

| Parameters | Value | Unit | Ref. |
|---|---|---|---|
| $B_1$ | $1 \times 10^{10}$ | m$^4$/kg s | This study [a] |
| $E_1$ | 120 | kJ/mol | [4] |
| $Q_1$ | $1.74 \times 10^4$ | kJ/kg | This study [b] |
| $B_2$ | $1 \times 10^{12}$ | m$^4$/kg s | This study [a] |
| $E_2$ | 190 | kJ/mol | [24] |
| $Q_2$ | $-1.44 \times 10^4$ | kJ/kg | [25] |
| $B_3$ | $3 \times 10^9$ | m$^3$/kg s | This study [a] |
| $E_3$ | 120 | kJ/mol | [4] |
| $Q_3$ | $1.01 \times 10^4$ | kJ/kg | [26] |
| $h_s$ | 10 | W/m$^2$K | [27] |
| $h_0$ | 30 | W/m$^2$K | [27] |
| $h_m$ | 0.01 | kg/m$^2$s | [28] |
| $\rho_c$ | 26.5 | kg/m$^3$ | [6] |
| $\rho_g$ | 1.2 | kg/m$^3$ | [4] |
| $c_g$ | 1006 | J/kg K | [29] |
| $R$ | $8.314 \times 10^{-3}$ | kJ/mol K | [30] |
| $S$ | $3.14 \times 10^{-4}$ | m$^2$ | This study [c] |
| $T_0$ | 300 | K | – |
| $V$ | $5.24 \times 10^{-7}$ | m$^3$ | This study [c] |

[a] Estimated in this study.
[b] Estimated based on the oxygen consumption method.
[c] Estimated based on the representative length of 1 cm.

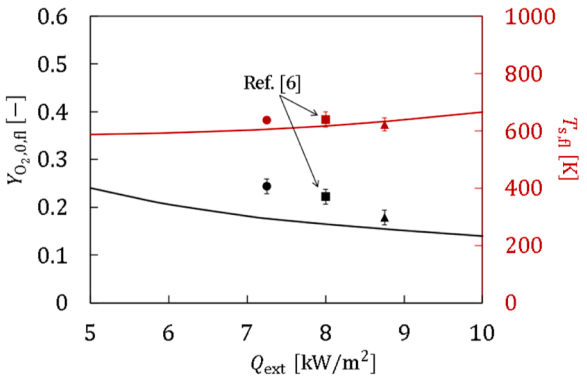


**Fig. 7.** Effect of external radiant heat flux ($Q_{ext}$) on the lower limit of oxygen mass fraction for flaming ($Y_{O_2,0,fl}$) and lower limit of surface temperature for flaming ($T_{s,fl}$). Solid lines: calculated results; ●, ■, ▲: experimental data [6]; $v_0^* = 4.2 \times 10^{-7}$ m$^3$/s.

surface area and air velocity, which are challenging to estimate. In this study, $h_s = 10$ W/m$^2$K is estimated using the relation $h_s = \lambda_g \mathrm{Nu}/d$, where Nu = 3.66 corresponds to the Nusselt number for laminar flow in the circular tube [27]. On the other hand, $h_0$ is more difficult to estimate due to the undetermined flow configuration. Therefore, we adopted a representative value, 30 W/m$^2$K, from a typical range of heat transfer coefficients, from 10 to 40 W/m$^2$K, based on values reported in the literature for natural convection [27]. A mass transfer coefficient of 0.01 kg/m$^2$s is estimated based on $h_m = \mathrm{Sh} D_g/d$ with the Sherwood (Sh) number of 4.36, corresponding to laminar flow in tubes under the assumption of a unity Lewis (Le) number (Le $= \alpha_g/D_g = 1$) [28]. The char surface area ($S$) and gas-phase volume ($V$) are estimated in this study based on a representative length of 1 cm, along with $S = \pi d^2$ and $V = \pi d^3/6$. A spherical geometry is adopted, considering the experimental conditions and for simplicity. However, the choice of $S$ and $V$ is arbitrary since the ratios of $SB_1\rho_c/\nu_0$, $SB_2\rho_c/\nu_0$, and $VB_3\rho_g/\nu_0$ are more significant, and adjusting $B_1$, $B_2$, and $B_3$ is necessary to reproduce the experimental data.

The effects of radiant heat flux ($Q_{ext}$) on the lower limit of oxygen mass fraction for flaming ($Y_{O_2,0,fl}$) and lower limit of surface temperature for flaming ($T_{s,fl}$) are investigated, as shown by the black and red solid lines in Fig. 7, respectively. The results indicate that the flaming ignition is more likely to occur in environments with higher radiant heat flux. At $Q_{ext} = 5$ kW/m$^2$, the flaming ignition occurs at $Y_{O_2,0,fl} = 0.24$, while under $Q_{ext} = 10$ kW/m$^2$, $Y_{O_2,0,fl} = 0.14$ is sufficient to trigger the ignition. Additionally, $T_{s,fl}$ increases with increasing $Q_{ext}$ from 587 K at $Q_{ext} = 5$ kW/m$^2$ to 666 K at $Q_{ext} = 10$ kW/m$^2$. This range represents the minimum critical temperature for the piloted flaming ignition. The symbols in Fig. 6 correspond to experimental data [6] obtained at various radiant heat fluxes. It can be seen that the model reasonably reproduces the experimental $Y_{O_2,0,fl}$ across different radiant heat flux conditions. However, the predicted $T_{s,fl}$ tends to increase, while the experimental data are nearly constant with a slightly decreasing trend. One possible reason is that in the experiment, it is difficult to identify the location of the maximum surface temperature. In Ref., [6], the surface temperature was measured at the midpoint of the sample (60 mm), which may not correspond to the point of highest temperature. In contrast, the experimental $Y_{O_2,0,fl}$ values can be accurately controlled using mass flow controllers.

Figure 8 shows the effect of oxidizer flow rate on the combustion mode using the parameters in Table 2 and based on an external heat flux of 8.75 kW/m$^2$. The experimental data corresponding to no flaming ignition and flaming ignition are plotted as open and filled symbols, respectively. All the experimental data of flaming ignition lie within the bistable regime, confirming the model's capability. The data point of no flaming ignition is slightly above the lower limit of the ambient oxygen

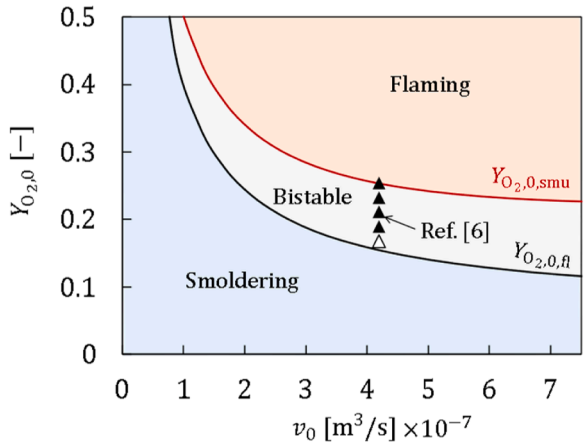


**Fig. 8.** Dependence of combustion mode on oxidizer flow rate ($v_0$) based on the parameters in Table 2. Experimental data [6] (△: no flaming ignition; ▲: flaming ignition).

mass fraction for flaming ($Y_{O_2,0,fl}$); the model underpredicts $Y_{O_2,0,fl}$, which is consistent with Fig. 7.

## 4. Conclusions

This study proposes a reduced model to predict the smoldering-to-flaming (StF) transition by considering surface (R1 and R2) and gas-phase (R3) reactions. The model assumes that the transition occurs when the surface temperature is sufficiently high to ignite the combustible gases. Various unknowns, including surface/gas-phase temperatures, reaction rates, and species concentrations, are solved simultaneously as part of the solution with pure smoldering, pure flaming, and combined cases.

The predicted results using dimensionless parameters show an increase in temperature with the oxygen mass fraction. The extinction of pure smoldering and flaming cases is estimated at the low oxygen mass fractions from the turning point of the solutions. Higher surface temperatures are observed in the pure smoldering case, while higher gas-phase temperatures are found in the pure flaming case. By considering the combined case, a shift from steady smoldering to steady flaming is observed, indicating the spontaneous StF transition.

The limit oxygen mass fraction of flaming, bistable, smoldering, and extinction regimes is simulated over a range of oxygen mass fractions and oxidizer flow rates. An important role of gas-phase temperature and CO mass fraction in triggering the transition is confirmed. The effect of heat loss is tested, showing the shift to a higher oxygen limit when increasing heat loss.

Lastly, the model is validated against experimental data, confirming a reasonable agreement. A decrease in the lower limit of oxygen mass fraction for flaming with increasing external radiant heat flux is revealed, while the lower limit of surface temperature for flaming remains within a certain range.

## Novelty and significance statement

The novelty of this research is the prediction of the limit conditions of smoldering combustion using a simplified model. This is the first time that the model successfully predicts the limiting conditions, e.g., smothering extinction, smoldering-to-flaming (StF) transition, as well as the steady-state solutions for both smoldering and flaming modes. This work is significant because the model not only bridges the knowledge gap between the distinct characteristics of smoldering and flaming combustion but also predicts the temperature, species concentrations, and limit conditions in each mode. While continuous research has studied the critical parameters triggering the transition phenomena, there remains a need for a simple yet widely applicable model to address this complex issue. This necessity highlights the significance of the model proposed in this study.

## CRediT authorship contribution statement

**Pichayaporn Viriya-amornkij:** Writing – original draft, Investigation, Formal analysis. **Kazunori Kuwana:** Writing – review & editing, Supervision, Project administration, Funding acquisition, Conceptualization. **Yasuhisa Saito:** Writing – review & editing, Methodology, Conceptualization. **Xinyan Huang:** Writing – review & editing, Methodology, Investigation, Conceptualization.

## Declaration of competing interest

The authors declare that they have no known competing financial interests or personal relationships that could have appeared to influence the work reported in this paper.

## Acknowledgments

A part of this work was supported by JSPS KAKENHI Grant Number JP21H04593. XH thanks the support from the National Natural Science Foundation of China (No. 52322610).

## Appendix A

The sensitivity analysis of model parameters in Table 2, such as $E_1$, $E_2$, $E_3$, $h_s$, $h_0$, and $h_m$, on the upper limit of surface temperature for smoldering ($T_{s,smu}$) is conducted as shown in Fig. A1, using parameters perturbed by up to ± 20 %. The results indicate that a change in $E_3$ has a greater impact on the critical $T_{s,smu}$, causing deviations of up to approximately 20 % under $a$ ± 20 % perturbation. These findings highlight the importance of gas-phase reaction (R3) in auto-StF behavior. Note that $B_3$ was not adjusted when $E_3$ was perturbed in this calculation. Some parameters in Table 2 were adjusted to match experimental data. In the future, more detailed kinetic analysis will be necessary for quantitative predictions.

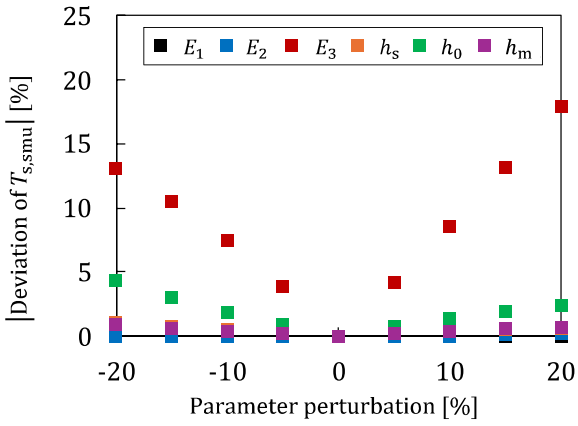


**Fig. A1.** Sensitivity analysis of parameters in Table 2 on $T_{s,smu}$.

## References


[1] T.J. Ohlemiller, Modeling of smoldering combustion propagation, Prog. Energy Combust. Sci. 11 (1985) 277–310.
[2] P. Viriya-amornkij, K. Kuwana, X. Huang, Predicting extinction limits of concurrent smoldering spread by a reduced analytical model, Combust. Flame. 269 (2024) 113668.
[3] S. Lin, T.H. Chow, X. Huang, Smoldering propagation and blow-off on consolidated fuel under external airflow, Combust. Flame 234 (2021) 111685.
[4] O. Kadowaki, M. Suzuki, K. Kuwana, Y. Nakamura, G. Kushida, Limit conditions of smoldering spread in counterflow configuration: extinction and smoldering-to-flaming transition, Proc. Combust. Inst. 38 (2021) 5005–5013.
[5] O. Putzeys, A. Bar-Ilan, G. Rein, A.C. Fernandez-Pello, D.L. Urban, The role of secondary char oxidation in the transition from smoldering to flaming, Proc. Combust. Inst. 31 (2007) 2669–2676.
[6] O.M. Putzeys, A.C. Fernandez-Pello, G. Rein, D.L. Urban, The piloted transition to flaming in smoldering fire retarded and non-fire retarded polyurethane foam, Fire Mater 32 (2008) 485–499.
[7] A. Bar-Ilan, O.M. Putzeys, G. Rein, A.C. Fernandez-Pello, D.L. Urban, Transition from forward smoldering to flaming in small polyurethane foam samples, Proc. Combust. Inst. 30 (2005) 2295–2302.
[8] F. Richter, F.X. Jervis, X. Huang, G. Rein, Effect of oxygen on the burning rate of wood, Combust. Flame. 234 (2021) 111591.
[9] Z. Zhang, P. Ding, S. Wang, X. Huang, Smouldering-to-flaming transition on wood induced by glowing char cracks and cross wind, Fuel 352 (2023) 129091.
[10] T.J. Ohlemiller, Forced smolder propagation and the transition to flaming in cellulosic insulation, Combust. Flame. 81 (1990) 354–365.
[11] S.D. Tse, A. Carlo, F. Nde-Pello, K. Miyasaka, Controlling mechanisms in the transition from smoldering to flaming of flexible polyurethane foam, Symp. Combust, Proc 26 (1996) 1505–1513.
[12] S. Alexopoulos, D.D. Drysdale, The transition from smouldering to flaming combustion, Fire Mater 13 (1988) 37–44.
[13] X. Huang, J. Gao, A review of near-limit opposed fire spread, Fire Saf. J. 120 (2021) 103141.
[14] A.B. Dodd, C. Lautenberger, C. Fernandez-Pello, Computational modeling of smolder combustion and spontaneous transition to flaming, Combust. Flame. 159 (2012) 448–461.
[15] J. Yang, N. Liu, H. Chen, W. Gao, Smoldering and spontaneous transition to flaming over horizontal cellulosic insulation, Proc. Combust. Inst. 37 (2019) 4073–4081.
[16] Y. Chen, Z. Liang, S. Lin, X. Huang, Limits of sustaining a flame above smoldering woody biomass, Combust. Sci. Technol. 195 (2023) 2801–2819.
[17] K. Sato, S. Sega, Mode of burning zone spread in an opposed gas flow, Combust. Flame. 83 (1991) 146–154.
[18] S. Sega, K. Sato, Study on smoldering-flaming transition of solid materials: concentration distribution of gases around char oxidation surface, J. Fire Sci. 3 (1) (1985) 26–34.
[19] T. Yamazaki, T. Matsuoka, K. Kuwana, Y. Nakamura, Study on the flaming-transition behavior of a downwardly smoldering biomass stick utilizing low pressure, Proc. Combust. Inst. 38 (2021) 5073–5080.
[20] R. Ganguli, V. Panchore, Stability analysis, in: R. Ganguli, V. Panchore (Eds.), The Rotating Beam Problem in Helicopter Dynamic, Springer, Singapore, 2018, pp. 83–91.
[21] N. Thinnakornsutibutr, K. Kuwana, M. Mizuno, T. Ushijima, S. Yazaki, Early warning signals of flashover in compartment fires, Fire. Saf. J 150 (2024) 104264.
[22] S.K. Aggarwal, Extinction of laminar partially premixed flames, Prog. Energy Combust. Sci. 35 (2009) 528–570.
[23] N. Peters, Laminar diffusion flamelet models in non-premixed turbulent combustion, Prog. Energy Combust. Sci. 10 (1984) 319–339.
[24] J. Gao, X. Qi, D. Zhang, T. Matsuoka, Y. Nakamura, Propagation of glowing combustion front in a packed bed of activated carbon particles and the role of CO oxidation, Proc. Combust. Inst. 38 (2021) 5023–5032.
[25] G. Adomeit, W. Hocks, K. Henriksen, Combustion of a carbon surface in a stagnation point flow field, Combust. Flame. 59 (1985) 273–288.
[26] D.D. Drysdale, Thermochemistry, in: M.J. Hurley, D. Gottuk, J.R. Hall Jr., K. Harada, E. Kuligowski, M. Puchovsky, J. Torero, J.M. Watts Jr., C. Wieczorek (Eds.), SFPE Handbook of Fire Protection Engineering, 5th Ed., Springer, New York, NY, 2016, p. 143.
[27] J.P. Holman, Heat Transfer, McGraw-Hill, New York, NY, 2010, p. 523.
[28] T.L. Bergman, A.S. Lavine, F.P. Incropera, D.P. Dewitt, Introduction to Heat Transfer, John Wiley & Sons, Inc., Hoboken, NJ, 2011, p. 510.
[29] J.R. Welty, C.E. Wicks, R.E. Wilson, G.L. Rorrer, Fundamentals of momentum, heat, and Mass Transfer, John Wiley & Sons, Inc., Hoboken, NJ, 2008, p. 541.
[30] S.Z. Miry, M.A.B. Zanoni, T.L. Rashwan, J.L. Torero, J.I. Gerhard, Investigation of multi-dimensional transfer effects in applied smouldering systems: a 2D numerical modelling approach, Combust. Flame 246 (2022) 112385.